

2D Computational Fluid Dynamics Simulation Analysis of the Assembly of Low-Temperature Cofired Ceramics/ Low-Temperature Cofired Ceramics and Si/Si Sandwiches by Reactive Bonding

Adam Yuile,* Alexander Schulz, Erik Wiss, Jens Müller, and Steffen Wiese

Numerical computational fluid dynamics simulations have been performed on 2D sandwich models to compare the performance of low-temperature cofired ceramics (LTCC)/LTCC and Si/Si sandwiches used in reactive bonding. In the sandwich model layers of solder, silver and a reactive multilayer used to bond the substrates are modeled. Additional to this, the surrounding air environment is also modeled. For simulating the heat released by the multilayer system, a user-defined function in the form of a square wave is written for the heat source with a defined width, corresponding to the reaction width, and this propagates at a fixed speed. Two sandwiches, one with LTCC/LTCC, and the other with Si/Si, are simulated and their response analyzed in terms of the solidification/melting of the solder and their respective time–temperature histories.

In recent times, there has been a growing interest in RMSs across various applications, notably in die bonding.^[4,5] This surge in interest stems from the essential need to integrate thermally diverse components^[6] (e.g., those with significantly different coefficients of thermal expansion) into specialized components while concurrently minimizing thermally induced stresses to uphold reliability.

On silicon-based substrates, the deposition of reactive multilayers has already been successfully implemented,^[7] but the intrinsic roughness of low-temperature cofired ceramics (LTCC) substrate technologies (in the range of 0.4–1 μm^[8–10]) makes this

deposition more difficult to achieve on LTCC technologies, despite the need and demand to diversify manufacturing technologies.^[11]

Conventional soldering techniques, like reflow soldering, mandate that all structures on a PCB must endure a heat cycle, a process which inflicts undesired stresses on the components.^[3] In contrast, RMSs allow the directed focus of heat sources onto specific localized areas.

Owing to the high-speed attributes of these RMSs and the innate nature of their propagation, during bonding, it becomes an ideal ground for simulation technology to be applied.^[1] This technology represents one of the most advanced simulation methodologies.

While simulation methods in electronic packaging have primarily focused on electrical, thermal, and thermomechanical issues during the operation of assemblies, the simulation of joining processes, particularly reactive bonding, is still developing. Simulations of reactive bonding processes often use finite-element/volume methods to model heat flow in multilayer substrates.

For instance in ref. [12], a cylindrically symmetrical grid has been used to approximate temperature distributions and reaction front velocities, assuming the propagation direction of the reaction front. Other simulation approaches, such as ref. [13], make use of 2D finite-element models that simulate the temperature and solder melting/solidification progression, albeit for different types of substrates, namely copper.


Further to this, in this article, the emphasis is very much placed on LTCC/LTCC and Si/Si bonding and comparing the performance of the two different substrate types/combinations. The vast majority of previous investigations in the RMS bonding

1. Introduction

Reactive multilayer systems (RMSs), used for bonding interconnects, prove highly effective for nanoscale film materials, such as Ni/Al, which contain stored chemical energy.^[1] Subsequent to ignition, for example, via a spark, these layers bond, releasing substantial energy as heat which allows the system to self-propagate.^[2] This exothermic heat release can then be used for melting solder paste to achieve localized soldering of heat-sensitive components,^[1] as an example, which downstream from the melting phase could then help form a permanent bond, upon solidification.^[3]

A. Yuile, E. Wiss, S. Wiese
Chair of Microintegration and Reliability
Saarland University
Saarbruecken 66123, Germany
E-mail: adam.yuile@uni-saarland.de

A. Schulz, J. Müller
Faculty of Electrical and Computer Engineering
Department of Electronics Technology
TU Ilmenau
Ilmenau 98693, Germany

 The ORCID identification number(s) for the author(s) of this article can be found under <https://doi.org/10.1002/adem.202302283>.

© 2024 The Author(s). Advanced Engineering Materials published by Wiley-VCH GmbH. This is an open access article under the terms of the Creative Commons Attribution License, which permits use, distribution and reproduction in any medium, provided the original work is properly cited.

DOI: 10.1002/adem.202302283

field have almost always been related to the joining exclusively of silicon to silicon,^[7,14–16] metal to metal^[17,18] and silicon to metal.^[19] With respect to the reactive bonding process, there are two major differences, first the thermal conductivity and, second, the surface roughness. The thermal conductivity of an LTCC substrate is orders of magnitude lower than those of silicon and copper. Owing to the high aforementioned intrinsic LTCC roughness, the deposition of reactive nanolayers leads to a very different structure of the RMS compared to the smooth surfaces of silicon and metal substrates; hence, the behavioral differences are likely to be important and warrant significant investigative effort.

2. Computational Fluid Dynamics Model

To study the performance differences between Si/Si, case (i), and LTCC/LTCC, case (ii), sandwiches, a new 2D model was made using the ANSYS Workbench 2023R2 software, in contrast to the 3D models that were previously studied.^[20] This meant that the models are principally similar to other 2D analyses, e.g.,^[13] only that the air surrounding the solid bodies is also modeled and therefore no convection boundaries are prescribed on the solid boundaries.

In this new 2D model, a domain with extents of 10 × 5 mm was modeled, in which a centrally located sandwich model, 4 mm in length, of either Si/Ag/solder/RMS/solder/Ag/Si, case (i), or LTCC/Ag/solder/RMS/solder/Ag/LTCC, case (ii), was housed.

In LTCC technology, the intrinsic surface roughness, and the scatter thereof, are known to affect the RMS behavior in ways that are not similarly suffered for by Si substrates. However, for simplicity of direct comparison, all layers are present in both cases and even the same substrate thicknesses are used, despite Si substrates tending to be thinner.

Table 1. Model layer thicknesses, for case (i) and (ii).

	Layer thickness [μm]
LTCC/Si	800
Ag	5
Solder	5
RMS	10

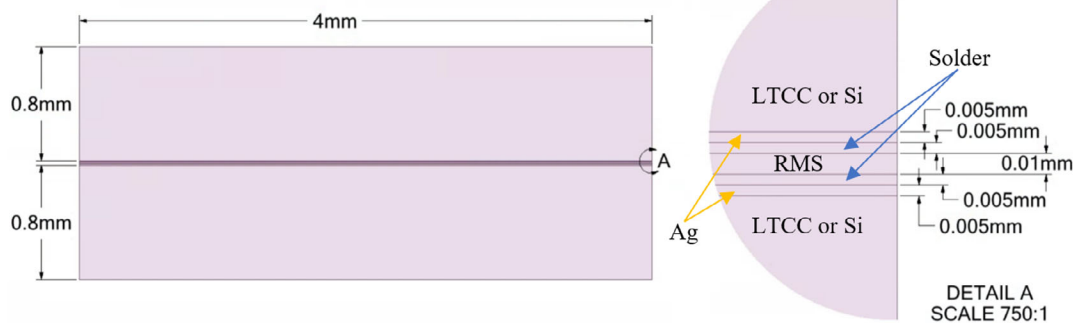


Figure 1. 2D CFD sandwich model dimensions, case (i) and (ii), with detail A highlighting 750:1 view of thin layers, and Ag, with Ni/Al RMS and solder layers highlighted.

The computational fluid dynamics (CFD) model extent of 10 × 5 mm was considered large enough to mitigate any significant influence of the external boundaries on the progression of the reaction. The respective model thicknesses being as per **Table 1**.

These same model thicknesses are also shown in **Figure 1**, with a detailed view of the thin layers (DETAIL A) also presented on the right.

The RMS, approximating an Ni/Al-based system, was effectively ignited from the left of the sandwich and the exothermic heat release propagated in the positive x direction, based on a square wave function, as per Equation (1). The propagation velocity is 5 m s^{-1} , a typical value for RMS propagation on LTCC, without pretreatment.^[21] C is a constant, of magnitude 1.44×10^5 , u is the velocity, w_r the reaction width, and Δt the time step

$$P = \frac{C}{uw_r \Delta t} \quad (1)$$

This volumetric power density, P , was only nonzero out with the bounds of the reaction, which started at the leading edge and moved, consistent with the reaction width and reaction velocity, in the positive x direction. The output of these functions would supply the 2D model with a volumetric power density, effectively as a heat input function, which was assumed to be equivalent to the exothermic heat released by the RMS, differing from the previous probability density-function-based approach.^[22]

Table 2 shows the solid material properties that were used for the LTCC—GreenTape DuPont DP951, Si, Ag, and RMS—corresponding to a non-reacted layer,^[13] where the Si and Ag material properties are sourced from ANSYS Fluent material databases. These parameters were assumed to be constant values, which could be improved upon in future work, given that the temperature variations are large and significant disparities in material properties could be present.

The air in the CFD model, which envelops the solid structures, has density of 1.225 kg m^{-3} , thermal conductivity of $0.0242 \text{ W m}^{-1} \text{ K}^{-1}$, and a specific heat capacity of $1006.43 \text{ J kg}^{-1} \text{ K}^{-1}$. A coefficient of expansion of 0.0034 K^{-1} is used for air, through the Boussinesq approximation, to estimate air buoyancy effects caused by temperature gradients, with

Table 2. Solid material properties for CFD model, based on ANSYS fluent material database, GreenTape DuPont DP951 data sheet, and non-reacted nanofoil.^[13]

	ρ [kg m ⁻³]	k [W m ⁻¹ K ⁻¹]	C_p [J kg ⁻¹ K ⁻¹]
LTCC	3100	3.3	600
Si	2500	710	100
Ag	10 490	234.28	419.97
Ni/Al RMS ^[13]	5500	152	830

respect to a gravitational acceleration of 9.81 m s⁻² enacting body forces on the air.

To model solder transitions between the liquid/molten and solid state, and the accompanying latent heat, the melting/solidification model was turned on in ANSYS Fluent. The melting/solidification model in ANSYS Fluent makes use of an enthalpy–porosity approach which provides an indication of the fraction of a cell volume that is in the molten state, where a liquid fraction of 0 corresponds to the solid state and, likewise, a liquid fraction of 1 the molten state. The pure solvent melting heat for the solder is 58.5 kJ kg⁻¹. And, 217 and 220 °C were given as the liquidus and solidus temperatures of the solder, thermal properties that closely resemble a typical SAC (tin–silver–copper) solder. The solder was specified to have density of 7000 kg m⁻³, specific heat capacity of 230 J kg⁻¹ K⁻¹, thermal conductivity of 63.2 W m⁻¹ K⁻¹, and dynamic viscosity of 0.1 Pa s⁻¹.

All of the aforementioned solid and fluid structures were meshed using ANSYS Workbench 2023R2, by applying a similar approach to that previously utilized.^[22] The mesh was 1 800 000 cells in size with edge lengths of 1.6667 and 16.667 μm in the vertical and horizontal directions. These mesh specifications corresponded to a minimum of three elements throughout the thickness of the thinnest structures—i.e., that of the Ag metallization, leading to a standard cell aspect ratio of 10:1.

On the left boundary, a velocity inlet of 0.1 m s⁻¹, with 5% turbulence intensity and turbulence viscosity ratio of 10, was used with a pressure outlet boundary on the opposite side having identical turbulence properties and a gauge pressure of 0 Pa.

Heat transfer within the domain, including between solid structures and air, is accounted for through the implementation of coupled boundaries in combination with the energy equation. The energy equation is solved numerically in ANSYS Fluent, together with the continuity, and x - and y -momentum equations for 10 000 individual time steps, with a fixed time step increment of 10⁻⁶ s.

Using 32 cores to solve numerically, convergence was attained for all 10 000 time steps, using default convergence criteria and under-relaxation factors. The initial time steps required on the order of 50 iteration cycles to converge, thereafter convergence was achieved in a handful of iterations, for each time step.

3. Results

Here, the results are presented and compared for the two aforementioned cases, namely case (i) with Si/Si sandwich and case (ii) with LTCC/LTCC sandwich. First, to use an appropriate amount of heat as input, comparisons between experimental measurements presented in ref. [20] made on 10 μm Ni/Al RMS deposited on pure LTCC (Experiment 1) and titanium metallization + laser structuring (Experiment 2) and an additional CFD model were made for different reaction widths—100, 300, and 900 μm, where the temperature contour results are shown in **Figure 2** and the time–temperature progression at a measuring point on the symmetry line inside the RMS (2 mm downstream from reaction initiation location) in **Figure 3**.

The temperature contours, shown here 0.4 ms after reaction initiation in **Figure 2**, demonstrate the reaction moving in the positive x direction with wider temperature contours being left in the wake of the reaction and a tight temperature peak in the reaction zone. Note due to the thin, high aspect ratio nature of the RMS, and other structures that only the first 2 mm of the sandwich is displayed, concentrated toward the leading edge of the domain. This holds true for subsequent plots of temperature and liquid fraction contours.

In **Figure 4**, a zoomed-in view of that of **Figure 2** shows the temperature contour levels in more detail, together with a scale which shows that the highest temperature band (880–975 °C) after 0.4 ms covers an area wider than 100 μm (approximately half of the reaction width—150 μm) and is limited to the

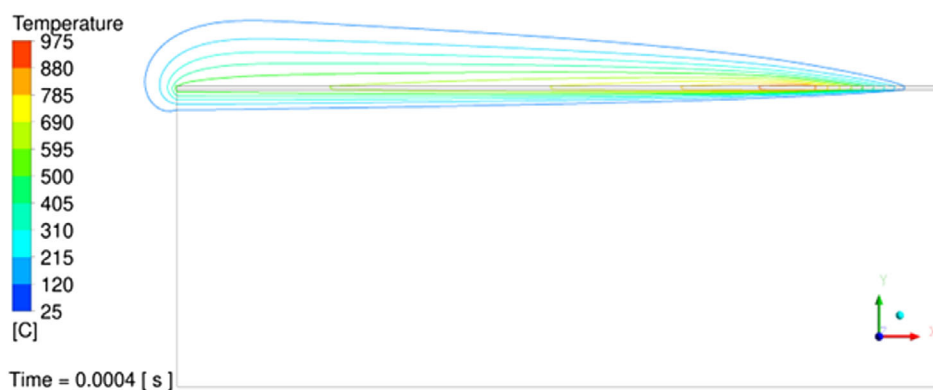


Figure 2. Temperature contours 0.4 ms after reaction initiation for 10 μm Ni/Al RMS deposited on 800 μm LTCC substrate with 300 μm RMS reaction width.

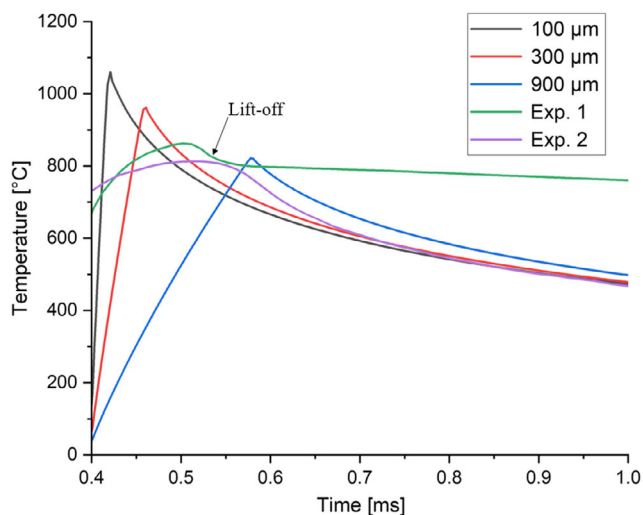


Figure 3. Square wave function reaction width variation (100, 300 and 900 μm) versus experimental pyrometer measurements for 10 μm Ni/Al RMS on pure LTCC substrate. Exp. 1 = 10 μm Ni/Al RMS deposited on pure LTCC, Exp. 2 = titanium metallization + laser-structure treatment.

thickness of the RMS, less a slight incursion into the air above the RMS. Even with a zoomed-in view focused on the reaction area, it is observed that the contour bands are very tight inside the LTCC, and thus the temperature gradients are very strong.

It was hypothesized in the experimental measurements of Figure 3 that liftoff, as highlighted on the figure, occurred during the pyrometer measurements^[20] of experiment 1—owing to the inadequate adhesion of RMS deposited on pure LTCC, so the temperature data there should be interpreted with some caution. That said, a reaction width of around 300 μm was found to offer a sensible match, both in terms of peak temperature attained and temperature decay rate, post-peak. The influence of this suspected liftoff of the 10 μm Ni/Al RMS deposited on LTCC is further demonstrated with experimental configuration 2, for an LTCC with titanium metallization and laser-structured treatment to improve adhesion,^[20] where a closer match between the simulated and experimental results is obtained, albeit for a slightly different configuration.

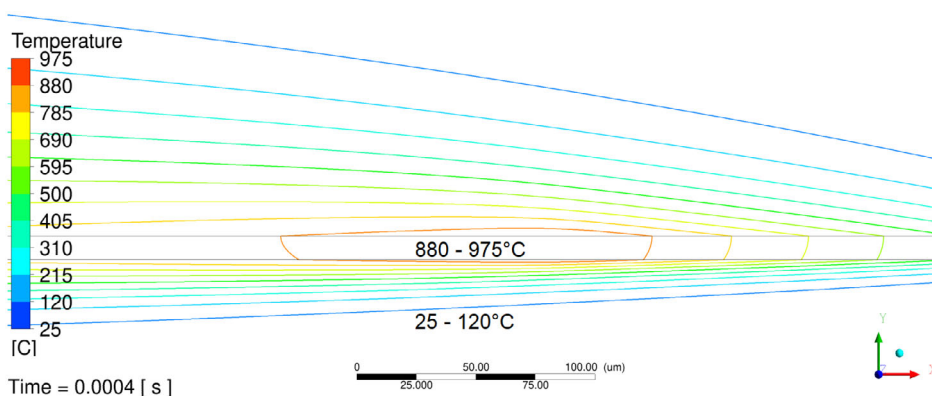


Figure 4. Zoomed-in temperature contour levels for 10 μm Ni/Al RMS on pure LTCC substrate, with highest and lowest contour levels highlighted.

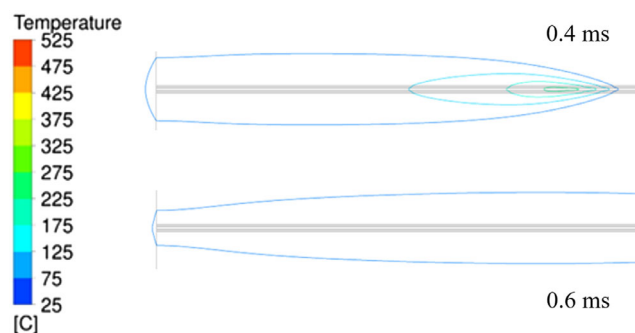


Figure 5. Temperature contours after 0.4 ms, case (i). Model assumptions: bottom substrate = Si, thickness = 800 μm, top substrate = Si, thickness 800 μm, joining zone: bottom and top surface layer = Ag, thickness 5 μm, Ni-Al RMS layer, thickness = 10 μm placed centrally between solder layers of 5 μm thickness.

Moving forward with a reaction width value for the square wave function of 300 μm, comparisons were then made between the performance of Si/Si, case (i), and LTCC/LTCC sandwiches, case (ii), in ANSYS Fluent, using the CFD modeling approach that has previously been described.

The temperature contours for the Si/Si sandwich are shown for 0.4 and 0.6 ms as shown in Figure 5. The peak temperatures are relatively modest and the spreading of the heat away from the bonding zone is observed to be quite effective, with all areas in the first 2 mm of the sandwich under 125°C by 0.6 ms.

In Figure 6, the liquid fraction contour plots are shown, also for 0.4 and 0.6 ms after reaction initiation. After 0.4 ms, a small region of molten solder, narrower even than the reaction width, is observed and this small bubble of molten solder has already been observed to have completely resolidified by 0.6 ms.

In Figure 7, the temperature contours at 0.4, 0.6, and 1.2 ms after reaction initiation are shown for case (ii). Comparing back to case (i), in Figure 5, for 0.4 and 0.6 ms, one can observe that the temperatures are significantly higher for the LTCC/LTCC sandwich, despite the same amount of energy being provided through the volumetric power density/heat source input function.

Furthermore, the temperature contour bands are much narrower, and this is because the heat is spread less effectively,

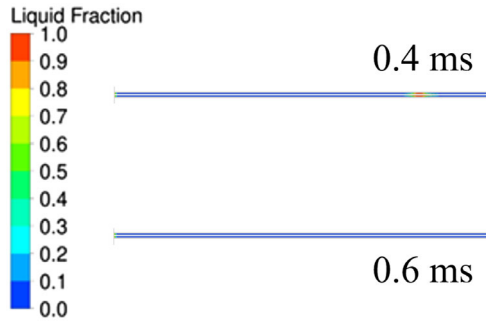


Figure 6. Liquid fraction contours for Si/Si sandwich after 0.4 ms (upper) and 0.6 ms (lower), case (i). Model assumptions: bottom substrate = Si, thickness = 800 μm , top substrate = Si, thickness 800 μm , joining zone: bottom and top surface layer = Ag, thickness 5 μm , Ni–Al RMS layer, thickness = 10 μm placed centrally between solder layers of 5 μm thickness.

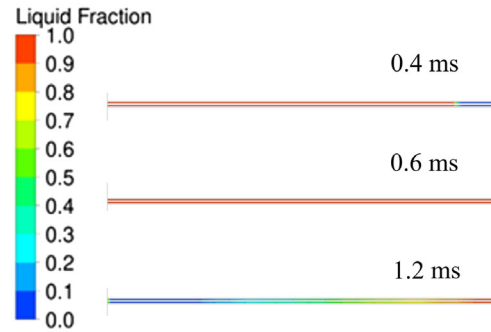


Figure 8. Liquid fraction contours for LTCC/LTCC sandwich after 0.4 ms (upper), 0.6 ms (center), 1.2 ms (lower), case (ii). Model assumptions: bottom substrate = LTCC, thickness = 800 μm , top substrate = LTCC, thickness 800 μm , joining zone: bottom and top surface layer = Ag, thickness 5 μm , Ni–Al RMS layer, thickness = 10 μm placed centrally between solder layers of 5 μm thickness.

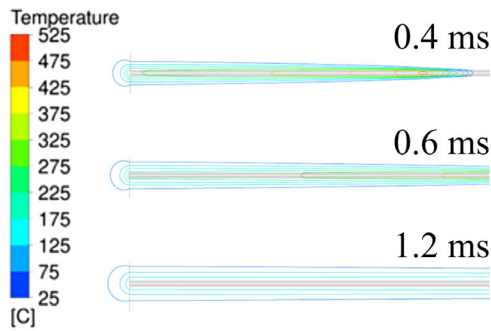


Figure 7. Temperature contours for LTCC/LTCC sandwich after 0.4 ms (upper), 0.6 ms (center), and 1.2 ms (lower) case (ii). Model assumptions: bottom substrate = LTCC, thickness = 800 μm , top substrate = LTCC, thickness 800 μm , joining zone: bottom and top surface layer = Ag, thickness 5 μm , Ni–Al RMS layer, thickness = 10 μm placed centrally between solder layers of 5 μm thickness.

owing to the low thermal conductivity of the LTCC material. This is particularly true for 1.2 ms where there is still much more significant elevated temperature inside the LTCC, long after this heat had already dissipated for the Si/Si case—case (ii).

These prolonged elevations in the local temperature in the bonding zone leave a pronounced influence on the liquid fraction contours. In **Figure 8**, the molten solder volume is orders of magnitude larger than in the Si/Si case of **Figure 6** at 0.4 ms post-ignition, to the extent that by 0.6 ms the entire solder in the region of interest is still in the molten state.

At 1.2 ms after reaction initiation, the solder in the LTCC/LTCC sandwich has started to resolidify and a bond can be successfully formed. In some cases, it may prove advantageous to have such a large percentage of the solder being molten concurrently, but from another perspective, it could highlight a lack of controlled precision with the method, in practice.

In **Figure 9**, direct graphical comparisons are made between the LTCC/LTCC and Si/Si sandwiches at several points in the models, all 2 mm downstream from leading edge at the center of the RMS, solder and at 5 μm depth into the substrate (Si or LTCC). The temperatures are clearly elevated by an additional

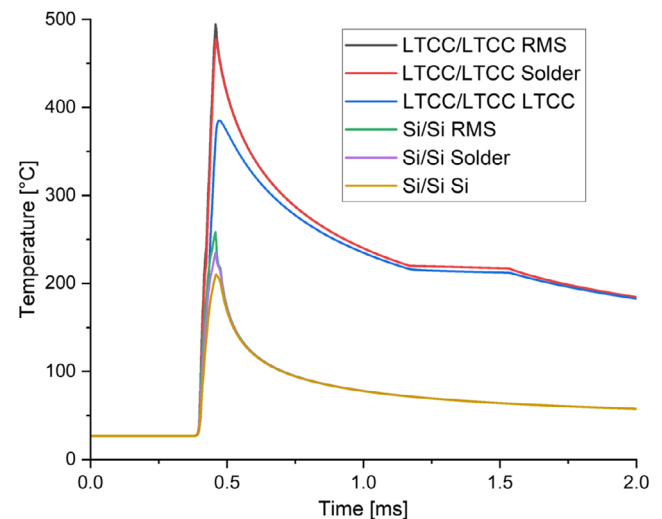


Figure 9. Comparisons between observed temperatures in the LTCC/LTCC versus Si/Si sandwiches in the RMS, solder and within the sandwiches themselves—at 5 μm depth into the substrates.

Table 3. Time for solder to reach peak temperature, solder liquidus, and solidus temperature.

Substrate combination	t_{peak}	t_{liquidus}	t_{solidus}
LTCC/LTCC	0.461	1.174	1.531
Si/Si	0.458	0.468	0.473

250 $^{\circ}\text{C}$ for the LTCC and the amount of time to achieve cooldown is also significantly longer. This is perhaps not ideal for bonding precision, and neither for the solder performance, but can help to reduce thermal shock.

These significant deviations, in not just thermal performance but also temporal differences, are highlighted in **Table 3**. In **Table 3**, it is clear to see that although the time from ignition to reach peak temperature does not differ significantly between

LTCC and Si, the time for the solder to cool back down to solder liquidus and solidus temperatures is significantly longer. Furthermore, while the time to cool down the 3 °C between the solder solidus and liquidus temperatures takes only 10 μs for Si/Si, this takes 357 μs for LTCC/LTCC, which is significantly longer and shows that the latent heat of the solder plays a much more noteworthy role for LTCC substrates.

4. Conclusion

While using LTCC substrates can bring many advantages, e.g., significant reductions in manufacturing cost relative to Si counterparts, the CFD simulation results show that the temperatures seen in LTCC/LTCC sandwiches are much higher than those in Si/Si. This is due to the lower thermal conductivity of the LTCC substrates and their relative inability to transport heat away from the bonding zone. Before this work, the temperature fields and solder progression were not studied in such detail for LTCC/LTCC.

Based on this CFD analysis, it was also highlighted that the latent heat of the solder plays a much more substantial role during the cooldown for the LTCC than the Si substrates, and that the time taken for the cooldown to transition between the solder liquidus and solidus temperatures was 35x greater for the LTCC substrates.

This extra heat could contribute to a longer than necessary melting phase of the solder, at much higher temperatures, which contribute to detrimental effects on the bonding performance as well as the increased impact, in terms of the stresses inflicted during the bonding necessitating the use of thicker solder layers to sustain these extra loads.

The question as to how to solve this remains uncertain, but perhaps using thicker solder pastes and more precisely calculated RMS deposition thicknesses could be an option based on these CFD simulation results. This analysis quantifies the severity of the issue to show the magnitude of the temperatures experienced in the bonding zone, which are extremely difficult to determine through experimental means.

Acknowledgements

This research work was supported by the Deutsche Forschungsgemeinschaft (DFG, German Research Foundation)—project ID 426204742.

Open Access funding enabled and organized by Projekt DEAL.

Conflict of Interest

The authors declare no conflict of interest.

Author Contributions

Adam Yuile: Formal analysis (lead); Investigation (lead); Writing—original draft (lead); Writing—review & editing (lead). **Alexander Schulz:** Data curation (equal). **Erik Wiss:** Formal analysis (equal); Funding acquisition (equal); Supervision (lead). **Jens Müller:** Funding acquisition (equal); Supervision (supporting). **Steffen Wiese:** Formal analysis (supporting); Writing—review & editing (supporting).

Data Availability Statement

Research data are not shared.

Keywords

computational fluid dynamics, low-temperature cofired ceramics, reactive multilayers, Si/Si

Received: December 31, 2023

Revised: July 12, 2024

Published online: September 19, 2024

- [1] D. P. Adams, *Thin Solid Films* **2015**, 576, 98.
- [2] K. Raić, R. Rudolf, P. Ternik, Z. Žunić, V. Lazić, D. Stamenković, T. Tanasković, I. Anžel, *Mater. Tehnol.* **2011**, 45, 335.
- [3] M. Mueller, J. Franke, in *2014 IEEE 16th Electronics Packaging Technology Conf. (EPTC)*, IEEE, Singapore **2014**.
- [4] H. Ji, M. Li, S. Ma, M. Li, *Mater. Des.* **2016**, 108, 590.
- [5] A. Syed-Khaja, C. Kaestle, M. Mueller, J. Franke, *Appl. Mech. Mater.* **2015**, 794, 320.
- [6] J. Braeuer, J. Besser, M. Wiemer, T. Gessner, in *2011 16th Int. Solid-State Sensors, Actuators and Microsystems Conf.*, IEEE, Beijing, China **2011**.
- [7] J. Braeuer, J. Besser, M. Wiemer, T. Gessner, *Sens., Actuators A* **2012**, 188, 212.
- [8] M. Matters-Kammerer, U. Mackens, K. Reimann, R. Pietig, D. Hennings, B. Schreinemacher, R. Mauczok, S. Gruhlke, C. Martiny, *Microelectron. Reliab.* **2006**, 46, 134.
- [9] H. Jantunen, T. Kangasvieri, J. Vähäkangas, S. Leppävuori, *J. Eur. Ceram. Soc.* **2003**, 23, 2541.
- [10] A. Bittner, A. Ababneh, H. Seidel, U. Schmid, *Appl. Surf. Sci.* **2010**, 257, 1088.
- [11] M. Glaser, S. Matthes, S. S. Riegler, J. Hildebrand, J. P. Bergmann, P. Schaaf, I. Gallino, in *Engineering for a Changing World: Proc.; 60th ISC, Ilmenau Scientific Colloquium*, Technische Universität Ilmenau, Ilmenau, Germany **2023**.
- [12] R. Masser, J. Braeuer, T. Gessner, *J. Appl. Phys.* **2014**, 115, 244311.
- [13] S. Liang, Y. Zhong, S. Robertson, A. Liu, Z. Zhou, C. Liu, in *2020 IEEE 70th Electronic Components and Technology Conf. (ECTC)*, IEEE, Orlando, FL **2020**.
- [14] K. Maekawa, K. Kodama, S. Miyake, T. Namazu, *Jpn. J. Appl. Phys.* **2021**, 60, SCCL15.
- [15] B. Boettge, J. Braeuer, M. Wiemer, M. Petzold, J. Bagdahn, T. Gessner, *J. Micromech. Microeng.* **2010**, 20, 064018.
- [16] K. Maekawa, S. Ito, T. Namazu, *Jpn. J. Appl. Phys.* **2020**, 59, S11L01.
- [17] J. Wang, E. Besnoin, A. Duckham, S. J. Spey, M. E. Reiss, O. M. Knio, T. P. Weihs, *J. Appl. Phys.* **2004**, 95, 248.
- [18] J. Matteau, in *Int. Symp. on Microelectronics, Int. Microelectronics Assembly and Packaging Society*, Andover, Hampshire **2011**.
- [19] H. Ji, Y. Qiao, M. Li, *Scr. Mater.* **2016**, 110, 19.
- [20] E. Wiss, A. Yuile, A. Schulz, J. Müller, S. Wiese, in *2023 24th Int. Conf. on Thermal, Mechanical and Multi-Physics Simulation and Experiments in Microelectronics and Microsystems (EuroSimE)*, IEEE, Graz, Austria **2023**.
- [21] A. Schulz, H. Bartsch, N. Gutzeit, S. Matthes, M. Glaser, A. Ruh, J. Mueller, P. Schaaf, J. P. Bergmann, S. Wiese, in *MikroSystem Technik Congress 2021*, VDE, Ludwigsburg, Germany **2021**.
- [22] A. Yuile, A. Schulz, E. Wiss, J. Müller, S. Wiese, *Appl. Sci.* **2022**, 12, 2397.